Competing magnetic anisotropies in exchange coupled bilayers with growth-induced orthogonal uniaxial axes

L. M. Álvarez-Prado,[1,*] S. M. Valvidares,[1,2] J. I. Martín,[1] and J. M. Alameda[1]
[1]*Departamento de Física, Facultad de Ciencias, Universidad de Oviedo, c/Calvo Sotelo s/n, 33007 Oviedo, Spain*
[2]*Lawrence Berkeley National Laboratory, Berkeley, California 94720, USA*
(Received 27 July 2007; revised manuscript received 5 November 2007; published 21 December 2007)

Magnetic anisotropy has been studied in YCo_2/YCo_2 amorphous bilayers with variable thickness and orthogonal in-plane uniaxial anisotropies of the individual layers induced in the sputtering growth. The study of the magnetization reversal and the effective magnetic anisotropy of the bilayers has been performed as a function of the relative strength of the competing individual-layer anisotropies by magneto-optical measurements and transverse bias initial susceptibility measurements. Analysis of the results on the basis of an analytical phenomenological model and micromagnetic simulations allows the interpretation of the observed behaviors; it reveals the presence of a region at the interface with a strongly reduced anisotropy as well as a nonmonotonic variation of the global effective anisotropy of the bilayer as a function of the top layer thickness.

DOI: 10.1103/PhysRevB.76.214419 PACS number(s): 75.70.Cn, 75.30.Gw, 75.50.Kj

I. INTRODUCTION

Magnetic anisotropy is one of the fundamental physical parameters that determine the magnetization reversal processes in exchange coupled multilayers. These magnetic materials have been studied for a long time, both theoretically[1] and experimentally,[2] as they present a wide variety of behaviors (giant magnetoresistance,[3] exchange bias,[4] enhanced interfacial magnetic coupling,[5] inverted hysteresis loops,[6] etc.) that are interesting from a fundamental point of view as well as for their applications in magneto-optical recording devices.[7] Interestingly, the variety of behaviors observed in exchange coupled multilayers is remarkably broadened when there are two competing anisotropies present in the samples. This has been recently illustrated by studies of the magnetization reversal as the ratio of the different anisotropy energies is varied in coupled multilayers with exchange bias,[8] the role of magnetoelastic and magnetostatic interactions in exchange-spring multilayers,[9] or multilayers where in-plane anisotropic layers are exchange coupled to out-of-plane anisotropic multilayers.[10,11]

On the other hand, both the origin and the dispersion of the anisotropy in polycrystalline and amorphous ferromagnetic layers have been investigated for a long time, as its good understanding is a fundamental issue in order to control the magnetic behavior of the samples. Several procedures are now well established that allow to grow thin layers with well-defined induced magnetic anisotropy, for example, by the application of an external magnetic field during the growth[12,13] or by oblique-incidence atom deposition,[14–17] where the origin of the anisotropy is related with shadowing effects and the adatom mobility.

In this work, amorphous YCo_2/YCo_2 bilayers with orthogonal in-plane uniaxial anisotropies have been fabricated in order to study the magnetization reversal and the effective magnetic anisotropy as a function of the relative strength of both competing individual-layer anisotropies. Two related physical questions have been analyzed. First, how is the definition of the growth-induced magnetic anisotropy of a layer influenced by its growth on top of a predeposited layer with a different (perpendicular) magnetic anisotropy? Second, is it possible to perform an experimental characterization and to provide a theoretical interpretation for the effective resultant magnetic properties of a system composed by two chemically identical layers but with their individual uniaxial anisotropy axes perpendicular to each other? It also includes the analysis of the possibility to tune the magnetic anisotropy of the samples from high values to very reduced ones. To address these questions, the study has been performed as a function of the relative thicknesses of the layers, and the magnetic anisotropy has been induced by the oblique incidence of the atoms during the deposition. Experimental results as well as analytical and micromagnetic developed models show a nonmonotonic variation of the effective anisotropy energy and a smooth rotation of the global easy axis when the thickness of the top layer is increased, and they also indicate the presence at the interface of a region with a strongly reduced anisotropy. Furthermore, these models provide the connection between the resulting effective magnetic properties of the composed bilayer system and those of the individual components.

II. EXPERIMENT

The amorphous YCo_2 films have been grown on glass substrates by magnetron cosputtering from pure yttrium and cobalt targets at a sputtering pressure of 10^{-3} mbar (with a base pressure of the order of 10^{-9} mbar).[6] Thin layers of Nb with a thickness of 5 nm are used as buffer and capping layers to avoid oxidation. During the deposition, the incidence of the atomic flux of cobalt is normal to the substrate, while that of the Y atoms is oblique with an angle of 36° respect to the substrate normal. Due to this oblique incidence, the amorphous YCo_2 films present a well defined in-plane uniaxial magnetic anisotropy which direction is perpendicular to the incidence plane of the atoms,[18] as it is sketched in Fig. 1. Typical hysteresis loops with the field applied along the easy and hard axes are shown in Fig. 2; in the first case, the samples present a square loop with coercive fields of the order of 20 Oe, while the loop for the field along

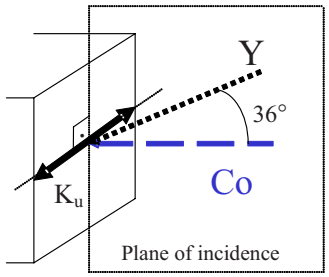

FIG. 1. (Color online) Sketch of the incidence of atoms in the deposition of YCo_2 layers.

the hard axis presents low remanence values and it is saturated at field values around 130 Oe.

The fabrication of the bilayers is performed in several steps. In the first one, the 5 nm thick Nb buffer layer is deposited on the substrate and then, on top of it, the first amorphous YCo_2 layer is grown with a thickness $t_1=10$ nm that is kept constant along the whole series of samples. After this deposition, the sample is rotated *in situ* 90° within the substrate plane (with a precision of ±5°) and then, the second YCo_2 magnetic layer is grown; in this way, the oblique incidence plane of the atoms is perpendicular to that of the deposition of the first YCo_2 layer and, therefore, it is expected an orthogonal configuration of the induced uniaxial anisotropies of both layers. The thickness of the top YCo_2 layer (t_2) has been varied between 10 and 110 nm. Finally, a Nb capping layer of 5 nm is grown on top of the samples. The amorphous character of the samples has been verified by x-ray diffraction, while the homogeneity of the chemical composition has been studied using x-ray microanalysis.[18] This analysis has shown a Co concentration of 66% along the samples, with a small deviation of +2% and −2% at the opposite edges of the large original 14×14 mm^2 substrate. In order to get a further limitation in the chemical homogeneity (below 1%), the magnetic measurements have been performed in rectangular samples with 5×10 mm^2 surface that have been cut from the central part of the original deposited larger samples.

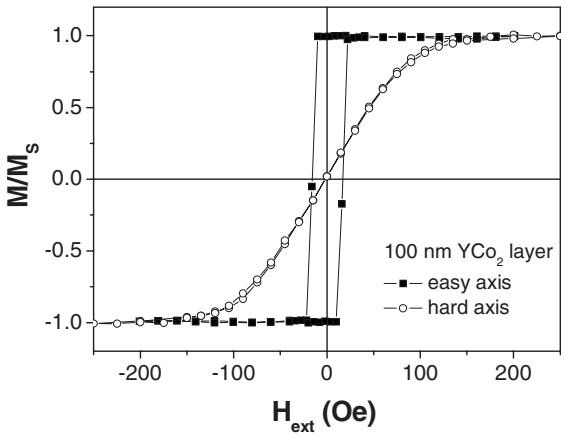

FIG. 2. Hysteresis loops with the field applied along the easy and hard axes of a YCo_2 film with a thickness of 100 nm.

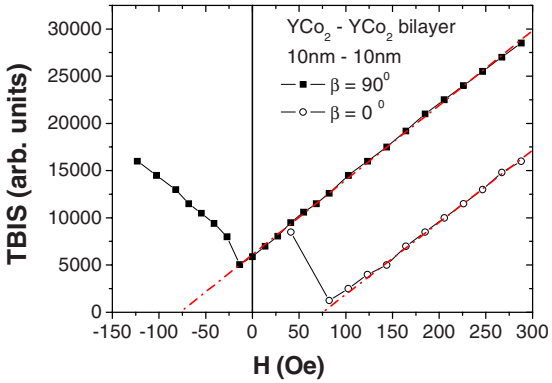

FIG. 3. (Color online) Transverse biased initial susceptibility $\chi_{t\beta}^{-1}$ versus H_{bias} for the 10 nm YCo_2/10 nm YCo_2 bilayer.

The magnetic properties have been analyzed by magneto-optical transverse Kerr effect (MOTKE) illuminating the samples with white light from the top layer side; it is known that, for Y-Co alloy films, the MOTKE signal is little dependent on the light wavelength in the visible range.[19] As the light penetration depth at these wavelengths is typically of the order of 40 nm,[20] it can be considered that the Kerr signal corresponds to the whole volume of the bilayer for $t_2 \leqslant 30$ nm, while for larger thicknesses, it corresponds mainly with the magnetic response of the top YCo_2 layer.

Also, the magnetic anisotropy of each bilayer has been obtained by transverse biased initial susceptibility TBIS $\chi_{t\beta}^{-1}$, applying the bias field (H_{bias}) in the parallel and perpendicular directions to the easy axis ($\beta=0°$ and $\beta=90°$, respectively).[21] The effective easy axis has been determined through the analysis of the behavior of the in-plane magnetization component that is perpendicular to the applied magnetic field.[22]

III. MAGNETIC ANISOTROPY OF YCo_2/YCo_2 BILAYERS

Figure 3 shows the experimental results of $\chi_{t\beta}^{-1}$ as a function of H_{bias} for the bilayer with $t_2=10$ nm. The curves present a very linear behavior for H_{bias} values larger than the one corresponding to the minimum in each curve. Thus, the anisotropy field H_K can be determined from the extrapolations of these linear dependences to the H_{bias} axis (as it is indicated with the dashed lines in the figure).[21] For an ideal uniaxial sample, these extrapolations should correspond with field values $\pm H_K$ for $\beta=0°$ and $\beta=90°$, respectively. The results of Fig. 3 reveal a well-defined uniaxial anisotropy as the intersections of both extrapolations at the H_{bias} axis are actually rather symmetric respect to zero field (the y axis). Slight asymmetries are usually observed in real samples, and they can be associated with effective field contributions that are related with the magnetization dispersion.[23] Then, H_K for each sample can be determined as the average of the two absolute values of χ_{t0}^{-1} and χ_{t90}^{-1} extrapolations to the H_{bias} axis.

Once the value of H_K has been evaluated, the magnitude of the anisotropy constant K_u can be determined by just considering the experimental saturation magnetization of YCo_2,

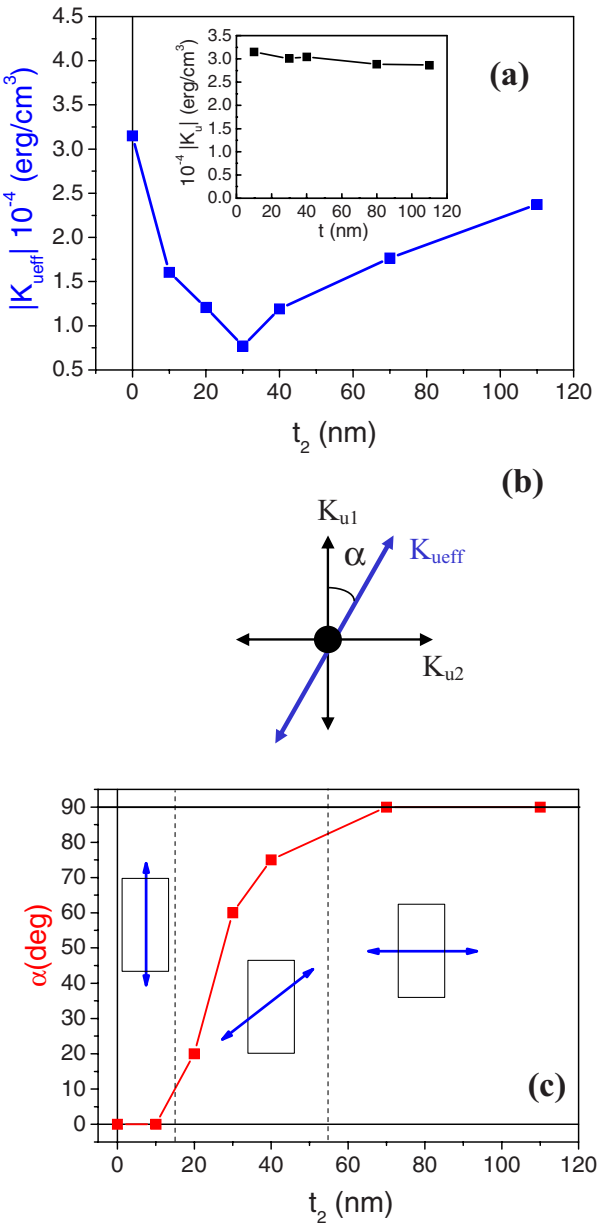

FIG. 4. (Color online) (a) Effective anisotropy $|\mathbf{K}_{ueff}|$ versus top layer thickness t_2 in the YCo_2/YCo_2 bilayers. Inset shows the thickness dependence of the anisotropy constant K_u in the YCo_2 single layers. (b) Sketch with the definition of the angle α associated with the effective anisotropy. (c) Thickness dependence of the angle α. Sketches with the direction of the effective anisotropy are included.

$M_S(YCo_2)=420$ emu/cm^3. In the case of YCo_2 single layers, the thickness dependence of K_u is shown in the inset of Fig. 4(a); the results present a very constant value of the anisotropy $K_u \sim 3\times 10^4$ erg/cm^3 with a slight decrease at high thickness values. It is worth noting that the magnitude of K_u and its thickness dependence vary with the configuration of the Y and Co sputtering targets.[18]

On the other hand, the behavior of the effective magnetic anisotropy of the YCo_2/YCo_2 bilayers is shown in Fig. 4. The magnitude of the effective anisotropy $|\mathbf{K}_{ueff}|$ presents a nonmonotonic behavior as a function of the second layer thickness, with a minimum at $t_2 \approx 30$ nm [see Fig. 4(a)]. These values have been obtained measuring from the air-sample side (similar results are obtained measuring from the substrate-sample side). Besides, the angle α between the direction of $\mathbf{K}_{ueff}$ and the direction associated with the growth-induced uniaxial anisotropy of the bottom YCo_2 layer [see sketch in Fig. 4(b)] shows a monotonic dependence [Fig. 4(c)] from $\alpha=0°$ (i.e., the direction associated with the uniaxial anisotropy of the bottom YCo_2 layer) to $\alpha=90°$ (i.e., the direction associated with the uniaxial anisotropy of the top YCo_2 layer); this last value is reached in bilayers with t_2 values larger than 40 nm. Also, the TBIS measurements at the minimum of $|\mathbf{K}_{ueff}|$ present asymmetric intersections with respect to zero field [Fig. 5(a)]; it corresponds with a clear increase in the remanence values in the hysteresis loops performed with the magnetic field applied perpendicularly to the $\mathbf{K}_{ueff}$ direction [Figs. 5(b) and 5(c)]. These TBIS and remanence results reveal that the sample presents a larger angular dispersion of the anisotropy axes, and it indicates that the effective uniaxial anisotropy of the bilayer is not so well-defined for these t_2 values.

IV. DISCUSSION AND MODELING

A. Phenomenological models with strongly coupled magnetizations

First, in order to analyze the experimental results, the discussion can start by considering the simplest phenomenological model. As it is well known,[6,24,25] if two strictly perpendicular uniaxial anisotropies ($\mathbf{K}_{u1}$ and $\mathbf{K}_{u2}$) act on the same magnetization of a bidimensional magnetic system, the Stoner-Wohlfart model predicts a resultant uniaxial anisotropy with a magnitude $|K_{u1}-K_{u2}|$ (being K_{u1} and K_{u2} the respective magnitudes of both perpendicular anisotropies) and a direction for the effective easy axis that is parallel to the one of the original uniaxial anisotropy with the highest magnitude. Then, to apply this model to the present results, it should be supposed that the exchange interaction at the interface is strong enough to align parallely the magnetization of both YCo_2 layers across the whole bilayer. Thus, according to this model and considering the smooth variation of the experimental uniaxial anisotropy values of the YCo_2 layers as a function of thickness [see inset of Fig. 4(a)], the deduced thickness dependence of the anisotropy of the YCo_2/YCo_2 bilayers would correspond with the one plotted in Fig. 6. It is evident that, although there are some general trends that are similar to the experimental data in Fig. 4, this kind of simple hypothesis is far of the quantitative agreement with the observed results. For example, in the framework of this model, the 10 nm YCo_2/10 nm YCo_2 bilayer should be isotropic and, also, the angle α of the effective anisotropy should not present a monotonic variation with t_2 but a sharp one.

For the case of strictly coupled magnetizations of both layers, it is easy to verify[6] that the monotonic variation of α with t_2 can only be justified if both individual anisotropies are not strictly perpendicular, which can be caused in real bilayers by experimental imprecision in the angular position of the substrate holder during growth. Taking into account this possible fact, the magnitude of the effective anisotropy

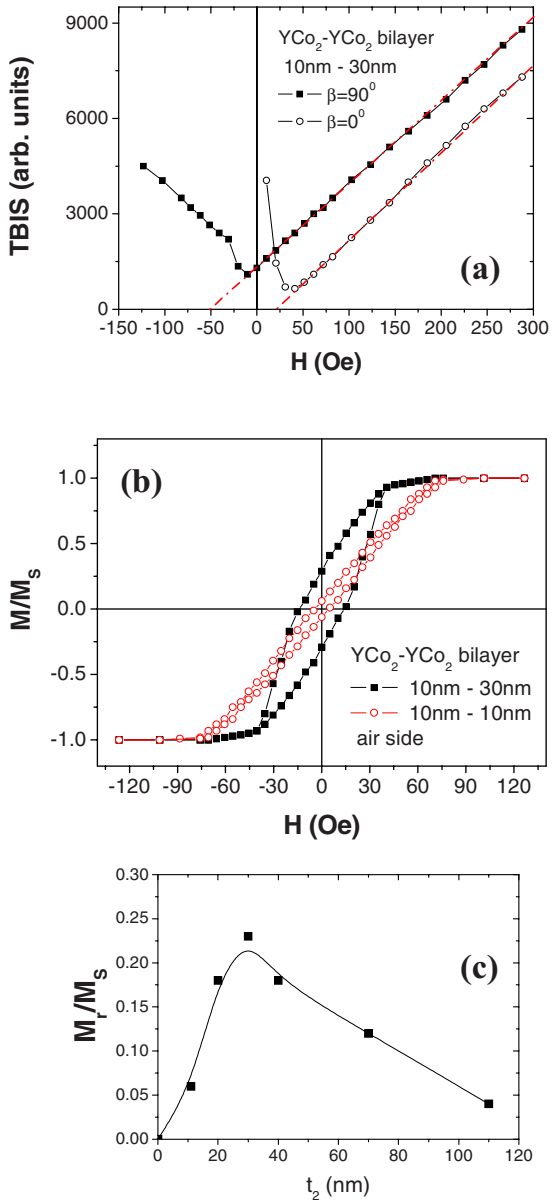

FIG. 5. (Color online) (a) TBIS measurements in YCo_2/YCo_2 bilayer with t_2=30 nm. (b) Hysteresis loops measured in bilayers with t_2=10 nm and t_2=30 nm for the field applied perpendicularly to the $\mathbf{K}_{ueff}$ direction. (c) Reduced remanence of the hysteresis loops measured as in (b) versus top YCo_2 layer thickness.

(K_{ueff}) and its angle α with respect to the direction $\mathbf{K}_{u1}$ can be written as[6]

$$(VK_{ueff})^2 = (V_1K_{u1})^2 + (V_2K_{u2})^2 + 2V_1V_2K_{u1}K_{u2}\cos(2\phi), \tag{1}$$

$$\cos(2\alpha) = [(VK_{ueff})^2 + (V_1K_{u1})^2 - (V_2K_{u2})^2]/2VV_1K_{ueff}K_{u1}, \tag{2}$$

where ϕ is the angle between both uniaxial easy axes and $V=V_1+V_2$, being V_1 and V_2 the respective volumes of each layer.

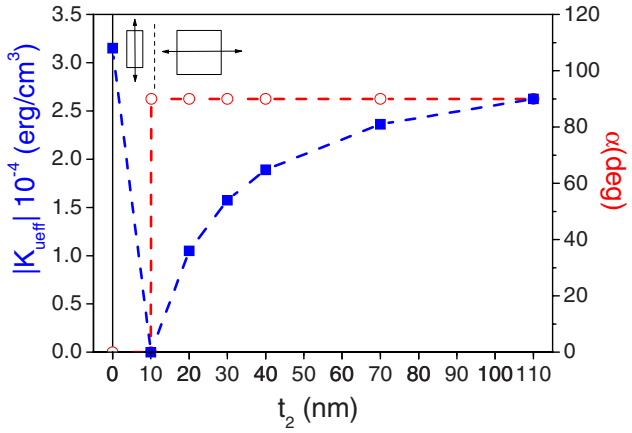

FIG. 6. (Color online) Thickness dependence of the effective anisotropy of the YCo_2/YCo_2 bilayers as deduced from the simplest phenomenological model of two strictly orthogonal uniaxial anisotropies acting on the whole magnetization.

Equations (1) and (2) can be summarized as

$$VK_{ueff}\cos(2\alpha) = V_1K_{u1} + V_2K_{u2}\cos(2\delta\varphi), \tag{3}$$

where $\delta\varphi$ is introduced to consider a possible small deviation of the perfect orthogonality between both uniaxial anisotropies (that is, $\phi=90°\pm\delta\varphi$). In order to compare with the experimental results, it is useful to particularize Eq. (3) for the exchange coupled bilayers, becoming

$$K_{ueff}\cos(2\alpha)(t_1+t_2) = K_{u1}t_1 - K_{u2}t_2[1-2(\delta\varphi)^2]. \tag{4}$$

Thus, if the experimental results are plotted as $K_{ueff}\cos(2\alpha)(t_1+t_2)$ vs t_2, a linear behavior would be obtained with a slope proportional to $K_{u2}[1-2(\delta\varphi)^2]$ and an intersection at $t_2=0$ of value $K_{u1}t_1$. However, as it is shown in Fig. 7(a), the experimental behavior does not correspond completely with the one of Eq. (4) as the dependence for small t_2 values is very different. Also, it is worth noting that, if the case $K_{u1}\equiv K_{u2}$ is supposed, the direction of the effective easy axis in the 10 nm YCo_2/10 nm YCo_2 bilayer should be close to $\alpha=45°$; however, the experimental result shown in Fig. 4(c) indicates that such anisotropy direction is still the same one of the bottom layer with a K_{ueff} value reduced to about the half of the one corresponding to the 10 nm YCo_2 single layer. This fact, together with the behavior observed at low t_2 values [Fig. 7(a)], suggests a reduction of the anisotropy in the top layers caused probably by the presence within the layer of a region with a reduced anisotropy.

To understand this reduction, it must be taken into account that the magnetic anisotropy of the top YCo_2 layer is finally the result of the competition between two different effects that act on the incoming atoms of the sample surface: first, the already mentioned anisotropic diffusion of the incoming atoms induced by the oblique incidence during the sputtering deposition that tends to align the uniaxial magnetic anisotropy along the direction that is perpendicular to the incidence plane of the atoms (see Fig. 1) and second, the exchange interaction with the atoms of the YCo_2 bottom

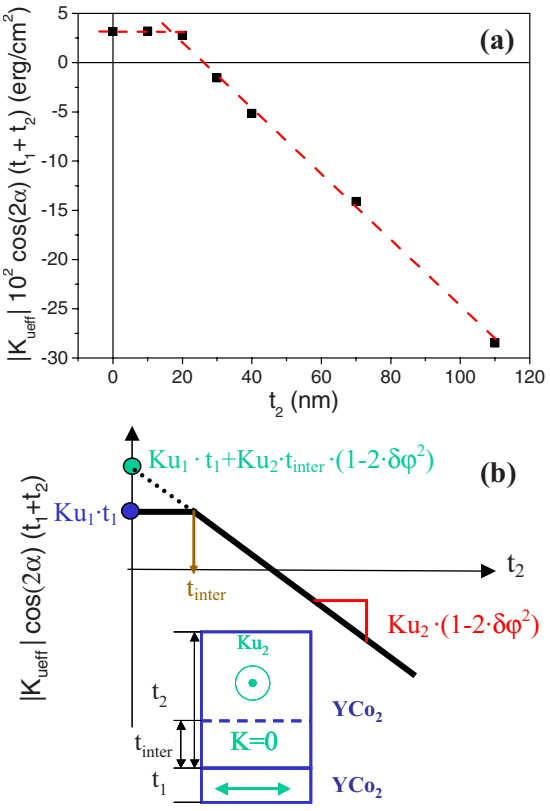

FIG. 7. (Color online) (a) Experimental behaviour of $K_{ueff}\cos(2\alpha)(t_1+t_2)$, anisotropy term in Eq. (4), as a function of top YCo_2 layer thickness. (b) Thickness t_2 dependence of the anisotropy term $K_{ueff}\cos(2\alpha)(t_1+t_2)$ as deduced from Eqs. (5a) and (5b); inset shows a sketch of the anisotropy configuration used to model YCo_2/YCo_2 bilayer experimental behaviour.

layer; as the sample is rotated 90° from its original growth position for the deposition of the top layer, the easy axis of the first YCo_2 layer and, as a consequence, its magnetization will be along the incidence plane of the atoms during the deposition of the second YCo_2 layer; therefore, the exchange interaction of the incoming atoms with the surface atoms of the first layer will tend to induce a similar spatial distribution in the second layer, that is, with the magnetization easy direction contained on the incidence plane of the incoming atoms. Thus, these competing perpendicular uniaxial effects of similar character can finally result in the presence of a region with a strongly reduced anisotropy.

Then, the simplest model to explain the results shown in Fig. 7(a) is to consider the existence of a region which anisotropy is essentially zero in the first steps of the growth of the top YCo_2 layer; after a certain thickness of the top layer (t_{inter}), the anisotropy would recover the value observed in the YCo_2 single layers. A sketch of the anisotropy in such modeling of the bilayer is shown in the inset of Fig. 7(b). With this hypothesis, the dependence of K_{ueff} as a function of the top layer thickness t_2 can be written as

$$K_{ueff}\cos(2\alpha)(t_1+t_2) = K_{u1}t_1 \quad \text{if } t_2 \leqslant t_{inter}, \tag{5a}$$

$$K_{ueff}\cos(2\alpha)(t_1+t_2) = K_{u1}t_1 - K_{u2}(t_2 - t_{inter})[1-2(\delta\varphi)^2] \quad \text{if } t_2 \geqslant t_{inter}. \tag{5b}$$

Figure 7(b) shows the thickness dependence contained in Eqs. (5a) and (5b), which presents a very good agreement with the experimental one obtained in Fig. 7(a). In particular, in a first approximation considering $K_{u1}=K_{u2}$, the fit of the experimental data to Eqs. (5a) and (5b) results in $t_{inter}=15$ nm, $K_{u1}=K_{u2}=10^4$ erg/cm^3, and $\delta\varphi \approx \pm 5°$.

B. Micromagnetic model with finite exchange coupling

Although the phenomenological model of the previous section has allowed us to explain in a first approximation the thickness dependence of the effective anisotropy K_{ueff}, it is not complete enough to describe the smooth variation of angle α with t_2 [see Fig. 4(c)]. Then, it is necessary to consider a micromagnetic model of the real sample, that is, where the exchange coupling between both layers is finite and, therefore, the magnetization is not strictly parallel across the whole thickness.

Thus, the real sample has been modeled by performing a unidimensional micromagnetic analysis,[26,27] where the magnetization profile across the thickness is represented by a chain of exchange coupled magnetic moments. Each of them corresponds to one of the 100 sublayers in which the whole sample is discretized along the thickness. The effective magnetic field acting on the magnetization of each sublayer has three contributions: the exchange interaction with its next neighbors, its Zeeman interaction with the external field, and its uniaxial anisotropy (for the micromagnetic modeling, the results obtained in Sec. IV A about the anisotropy are used in the discretization). In order to calculate the equilibrium states, the Landau-Lifshitz-Gilbert equation without precision term has been solved; the Runge-Kutta method of sixth order and with variable integration step has been used as the integration method. The initial state starts from a saturate configuration with the magnetic field applied in a certain direction (for example, the easy axis of the bottom layer) and, then, the profile of the magnetization across the thickness is calculated as the field is decreased without modifying its direction. The equilibrium condition is obtained when the maximum value of the torque $|\mathbf{u}_m \times \mathbf{H}|$ is 5×10^{-5} times the value of the magnetization (being $\mathbf{u}_m$ the unitary vector along the magnetization). Figure 8 shows the profile of the magnetization across the thickness obtained when the field has been reduced to zero for different thicknesses of the YCo_2/YCo_2 bilayer; in particular, the angle of the local magnetization [$\theta(t)$] with respect to the easy axis direction of the bottom YCo_2 layer (θ_{K1}) is represented for the case with parameters $A=7\times10^{-7}$ erg/cm,[28] $K_{u1}=K_{u2}=3\times10^4$ erg/cm^3, $M_S=420$ emu/cm^3, $t_{inter}=15$ nm (the shady region in the figure), and $\phi=80°$. For small values of the total bilayer thickness, i.e., for $t_1=10$ nm, the whole magnetization of the bilayer is parallel to the easy axis of the bottom layer. On the other hand, as the thickness of the top YCo_2 layer is increased, the global magnetization rotates continuously toward the easy axis of the second layer. The inset of Fig. 8 shows a rescaled

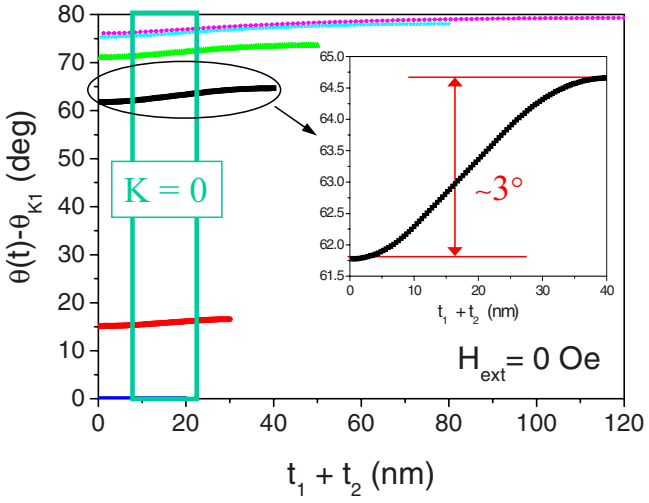

FIG. 8. (Color online) Micromagnetic simulated angular profiles of the magnetization across the thickness at $H=0$ for different values of the thickness t_2 of the YCo_2/YCo_2 bilayer; from bottom to top: $t_2=10$ nm (dark blue curve), $t_2=30$ nm (red curve), $t_2=40$ nm (black curve), $t_2=50$ nm (green curve), $t_2=80$ nm (cyan curve), and $t_2=120$ nm (pink curve). Inset shows a zoom of the magnetization angular profile for the 10 nm YCo_2/30 nm YCo_2 bilayer case.

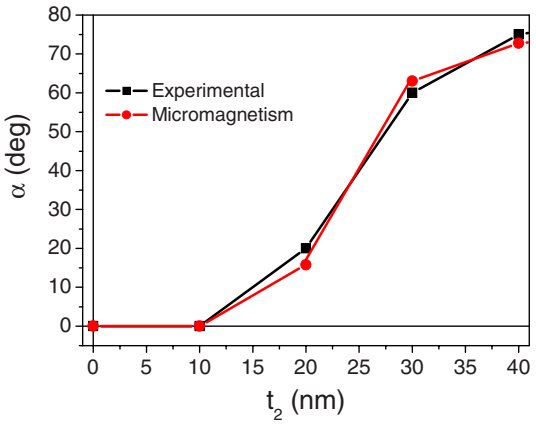

FIG. 9. (Color online) Comparison between the experimental (squares) and micromagnetic modeled (circles) results of the easy axis direction of the YCo_2/YCo_2 bilayers.

zoom of the profile of the magnetization for the 10 nm YCo_2/30 nm YCo_2 bilayer case; it indicates that the angular variation of the magnetization across the thickness is actually small (of the order of 3°), in reasonable agreement with the strongly coupled magnetization hypothesis considered in the analytical model of Sec. IV B. It has been checked that the obtained profiles are independent of the initial applied field direction.

Finally, it is worth comparing the experimental results of the easy axis direction of the bilayers obtained by MOTKE with the micromagnetic calculation ones, which are obtained for each bilayer as the average value of the magnetization angular profile represented in Fig. 8; in order to perform this average for the comparison, only the region of the top 40 nm of the bilayer (those closest to the sample-air interface) has been considered as it is this fraction of the bilayer what actually contributes to the experimental signal in the MOTKE measurements. Both kinds of results for the easy direction are compared in Fig. 9, revealing the good agreement between them and, therefore, indicating that the model is suitable for predicting the smooth variation as a function of thickness.

V. CONCLUSIONS

In summary, transverse Kerr effect and transverse bias initial susceptibility measurements combined with phenomenological and micromagnetic modeling have allowed us to determine the behavior of the magnetic anisotropy in YCo_2/YCo_2 exchange coupled bilayers; the uniaxial anisotropies of the individual layers are induced by the oblique incidence of the atoms during the deposition and are set to be perpendicularly aligned to each other. The main features of the magnetic anisotropy properties deduced from the analysis are the following.

(a) The results reveal the influence of the previous magnetic order of the bottom YCo_2 layer on the incoming atoms of the second YCo_2 layer deposited on top and, therefore, on its magnetic anisotropy. It is manifested in the presence of a region with a strongly reduced anisotropy at the interface of about 15 nm in thickness.

(b) The magnitude of the effective magnetic anisotropy of the whole bilayer presents a nonmonotonic behavior as a function of the top YCo_2 layer thickness, with a minimum for a value of about 30 nm (that is, a top layer three times thicker than the bottom one).

(c) The direction of the effective anisotropy rotates smoothly as a function of the top YCo_2 layer thickness; in particular, it has been found that the thickness of the top layer must be increased up to around 40 nm (that is, four times the thickness of the bottom layer) to reach the complete rotation from the bottom YCo_2 anisotropy direction to the top layer one.

(d) The micromagnetic results indicate that the whole magnetization across the thickness is actually well parallel to the effective anisotropy direction of the bilayer, presenting angular variations as small as 3°, in good agreement with the presence of a coupling between the magnetizations at the interface that is strong enough in the studied range of YCo_2 layers thickness.

These experimental and modeling results evidence the interest of an approach to the tailoring of magnetic properties based on systems composed by amorphous magnetic thin films with well-controlled magnetic anisotropies.

ACKNOWLEDGMENTS

Work supported by Spanish CICYT (Grant No. FIS2005-07392). Additional funding from the Spanish "Organismos Internacionales" and MEC/Fulbright grants (S.M.V.) is also acknowledged.

*lmap@uniovi.es

[1] E. Goto, N. Takaaki, T. Miyashita, and K. Nakagawa, J. Appl. Phys. **36**, 2951 (1965); H. Chang, Y. S. Lin, and A. Priver, *ibid.* **38**, 2294 (1967).
[2] W. T. Siegle, J. Appl. Phys. **36**, 1116 (1965); D. A. Thompson, L. A. Finzi, H. Chang, and P. Albert, *ibid.* **37**, 1274 (1966).
[3] S. N. Gordeev, J.-M. L. Beaujour, G. J. Bowden, B. D. Rainford, P. A. J. de Groot, R. C. C. Ward, M. R. Wells, and A. G. M. Jansen, Phys. Rev. Lett. **87**, 186808 (2001).
[4] J. Nogués and I. K. Schuller, J. Magn. Magn. Mater. **192**, 203 (1999), and references therein.
[5] D. Haskel, G. Srajer, J. C. Lang, J. Pollmann, C. S. Nelson, J. S. Jiang, and S. D. Bader, Phys. Rev. Lett. **87**, 207201 (2001).
[6] S. M. Valvidares, L. M. Álvarez-Prado, J. I. Martín, and J. M. Alameda, Phys. Rev. B **64**, 134423 (2001).
[7] X. Hu, Phys. Rev. B **55**, 8382 (1997).
[8] A. Paul, E. Kentzinger, U. Rücker, and T. Brückel, Phys. Rev. B **74**, 054424 (2006).
[9] H. D. Chopra, M. R. Sullivan, A. Ludwig, and E. Quandt, Phys. Rev. B **72**, 054415 (2005).
[10] J. Sort, V. Baltz, F. García, B. Rodmacq, and B. Dieny, Phys. Rev. B **71**, 054411 (2005); A. Bollero, L. D. Buda-Prejbeanu, V. Baltz, J. Sort, B. Rodmacq, and B. Dieny, *ibid.* **73**, 144407 (2006).
[11] G. Asti, M. Ghidini, R. Pellicelli, C. Pernechele, M. Solzi, F. Albertini, F. Casoli, S. Fabbrici, and L. Pareti, Phys. Rev. B **73**, 094406 (2006).
[12] G. Suran, K. Ounadjela, J. Sztern, and C. Sella, J. Appl. Phys. **55**, 1757 (1984); G. Suran, K. Ounadjela, and F. Machizaud, Phys. Rev. Lett. **57**, 3109 (1986).
[13] F. Luborsky, IEEE Trans. Magn. **13**, 853 (1977).
[14] T. G. Knorr and R. W. Hoffman, Phys. Rev. **113**, 1039 (1959); D. O. Smith, M. S. Cohen, and J. P. Weiss, J. Appl. Phys. **31**, 1755 (1960).
[15] S. L. Zeder, J.-F. Silvain, M. E. Re, M. H. Kryder, and C. L. Bauer, J. Appl. Phys. **61**, 3804 (1987).
[16] A. Lisfi and J. C. Lodder, Phys. Rev. B **63**, 174441 (2001); A. Lisfi, J. C. Lodder, H. Wormeester, and B. Poelsema, *ibid.* **66**, 174420 (2002).
[17] R. Morales, J. I. Martín, and J. M. Alameda, Phys. Rev. B **70**, 174440 (2004).
[18] L. M. Álvarez-Prado, R. Morales, and J. M. Alameda, J. Alloys Compd. **323-324**, 504 (2001); L. M. Álvarez-Prado, Ph.D. thesis, University of Oviedo, 1999.
[19] J. M. Alameda, M. C. Contreras, and A. R. Lagunas, J. Magn. Magn. Mater. **72**, 279 (1988).
[20] C. Dehesa-Martínez, L. Blanco-Gutiérrez, M. Vélez, J. Díaz, L. M. Álvarez-Prado, and J. M. Alameda, Phys. Rev. B **64**, 024417 (2001).
[21] J. M. Alameda and F. López, Phys. Status Solidi A **69**, 757 (1982).
[22] R. Morales, J. I. Martín, M. Vélez, and J. M. Alameda, Eur. Phys. J. B **40**, 463 (2004).
[23] K. Kempter and H. Hoffman, Phys. Status Solidi **34**, 237 (1969).
[24] E. J. Torok, H. N. Oredson, and A. L. Olson, J. Appl. Phys. **35**, 3469 (1964).
[25] S. Rinaldi and L. Pareti, J. Appl. Phys. **50**, 7719 (1979).
[26] M. Maicas, E. López, P. Sánchez, M. C. Sánchez, and C. Aroca, Phys. Rev. B **47**, 3180 (1993).
[27] G. Peral, J. L. Vicent, J. M. González, and D. Givord, IEEE Trans. Magn. **29**, 3108 (1993).
[28] B. Dieny, D. Givord, J. M. B. Ndjaka, and J. M. Alameda, J. Appl. Phys. **67**, 5677 (1990).